Design and Evaluation of a Control Scheme for the Hybrid Cascaded Converter in Grid Applications

Yu-Chen Su, *Student Member, IEEE*, Ping-Heng Wu, *Student Member, IEEE*, and Po-Tai Cheng, *Fellow, IEEE*

***Abstract*—Compared with the well-known modular multilevel cascaded converter with single-star bridge-cells (MMCC-SSBC), the hybrid cascaded converter (HCC) has the advantage of the lower component count of power transistors and dc capacitors. Thereby, this paper explores the HCC in grid applications and proposes a hierarchical control scheme, which allows the HCC to operate under unbalanced grid conditions and power imbalances among all cells. The HCC is further compared with the MMCC-SSBC under these unbalanced conditions to evaluate its performance. The laboratory test results are provided to verify the proposed control scheme and the comparison. The operational flexibility and reliability of the HCC are also discussed.**

***Index Terms*—DC capacitor voltage balancing control, grid applications, hybrid cascaded converter (HCC), power flow analysis, system current control, unbalanced conditions.**

I. Introduction

THE modular multilevel cascaded converter with single-star bridge-cells (MMCC-SSBC or SSBC) [1], as shown in Fig. 1(a), has attracted considerable attention in grid applications such as renewable energy systems (RES) [2]–[4], battery energy storage systems (BESS) [5], static synchronous compensators (STATCOM) [6]–[8], and so on. The dc capacitor voltage balancing control is an essential issue for the SSBC. A hierarchical control structure proposed in [9] has been proved as an effective method, which includes the overall control, the cluster control, and the individual control. Further study demonstrates that the dc capacitor voltage balancing can be attained even under unbalanced conditions by injecting the zero sequence voltage [10].

The main disadvantage of the SSBC is that a large number of power semiconductor devices are needed, which increases the number of gate signals and gate drivers as well. Besides, the existence of the double-frequency power ripple in each single-phase H-bridge cell makes the dc capacitance requirement higher. These drawbacks can be improved by integrating several single-phase H-bridge cells into one three-phase two-level cell, which lowers not only the component count, but also the dc capacitance requirement [11]. Accordingly, the topology of the hybrid cascaded converter (HCC), as shown in Fig. 1(b), is developed [12]–[16].

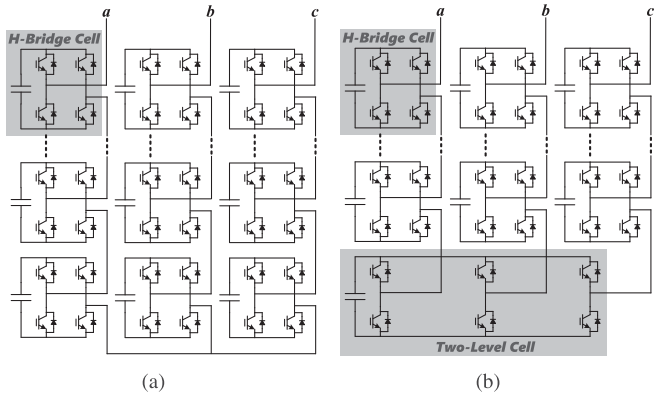

Fig. 1. Topologies of the SSBC and the HCC. (a) SSBC. (b) HCC.

The HCC is studied for electrical drives in [12] and [13], in which the two-level cell operates in square wave mode with higher voltage and the H-bridge cells operate in pulsewidth modulation (PWM) mode with lower voltage in order to optimize the system efficiency and the voltage levels. However, lots of isolated dc sources are indispensable for the HCC in electrical drives applications, which may lead to the difficulty in practical implementation. As a result, the HCC with the isolated dc sources replaced by floating capacitors is then studied for the grid-connected systems such as the high-voltage dc transmission [14] and the power rectifier [15], and all the floating capacitors can be kept at the desired voltages by means of the PI-based regulators [14] or the hysteresis-based regulators [15].

The HCC with the cells connected with floating capacitors may also be a promising candidate for such grid applications as RES, BESS, STATCOM, etc., but it has not been discussed until now [16]. The operation of these grid applications under unbalanced conditions is very important owing to the possibility of unbalanced conditions at dc-side, power imbalances among the cells, or ac-side, unpredictable grid faults, whereas it is not addressed in [12]–[15] because the system operations are based on balanced conditions.

In this paper, a control scheme is proposed for the HCC in grid applications. The proposed control scheme begins with a thorough power flow analysis on the HCC, and it is then designed following the hierarchical control structure developed in [9], while one more control, hybrid control, is added, becoming a

Manuscript received December 21, 2018; revised March 30, 2019 and May 17, 2019; accepted July 3, 2019. Date of publication July 8, 2019; date of current version December 13, 2019. This work was supported by the Ministry of Science and Technology, Taiwan, under Grant MOST 106-2221-E-007-065-MY3. Recommended for publication by Associate Editor L. Peng. *(Corresponding author: Yu-Chen Su.)*

The authors are with the Department of Electrical Engineering, National Tsing Hua University, Hsinchu 30013, Taiwan (e-mail: max970308@gmail.com; super497415008@gmail.com; ptcheng@ieee.org).

Color versions of one or more of the figures in this paper are available online at http://ieeexplore.ieee.org.

Digital Object Identifier 10.1109/TPEL.2019.2927601

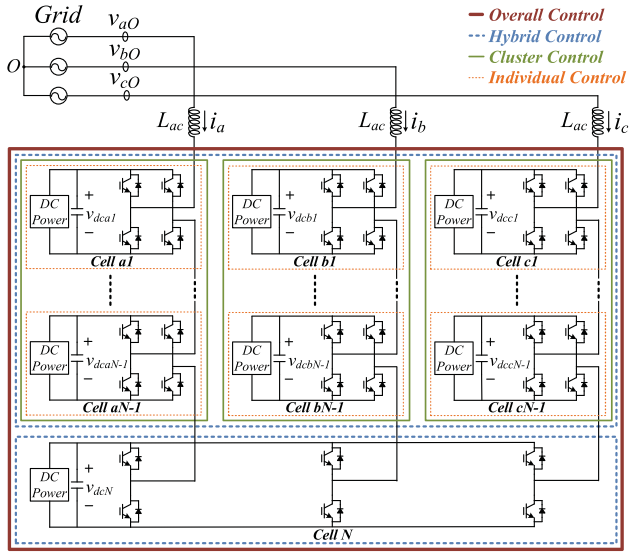

Fig. 2. System configuration of the HCC in grid applications.

four-layer hierarchical control scheme. Considering the unbalanced conditions, the proposed control scheme uses the zero sequence voltage as the means for managing the unbalanced power flows. Therefore, the proposed control scheme can achieve both the system current control and the dc capacitor voltage balancing control no matter the system is balanced or unbalanced. The HCC is further compared with the SSBC under the unbalanced conditions at dc-side or ac-side to evaluate its performance. The proposed control scheme and the comparison are both confirmed experimentally. Finally, the operational flexibility and reliability of the HCC are also carefully discussed.

II. System Configuration

Fig. 2 shows the system configuration of the HCC in grid applications, which is advantageous from the dimensioning point of view [11]. The HCC consists of $N-1$ H-bridge cells at each phase and one two-level cell, whose cascaded cell number can be adjusted depending on the system requirement. Each cell is connected with a dc power. Note that the dc powers can be renewables for RES or batteries for BESS, or even absent for STATCOM. The four-layer hierarchical control structure adopted in this paper is also shown in Fig. 2, which will be explained in detail in Section IV.

For the sake of controlling all the dc capacitor voltages accurately, the dc capacitor voltages of the H-bridge cells ($v_{\mathrm{dc}mn}$, $m = a, b, c$; $n = 1,..., N-1$) and the two-level cell ($v_{\mathrm{dc}N}$) are sensed and processed by the moving average filters to extract the average values [6]. Thereupon, the average dc capacitor voltages of the H-bridge cells ($V_{\mathrm{dc}mn}$, $m = a, b, c$; $n = 1,..., N-1$) and the two-level cell ($V_{\mathrm{dc}N}$) can be obtained. The dc voltage ratio of the H-bridge cells to the two-level cell is set as $1{:}K$ in this paper, namely, $V_{\mathrm{dc}N} = KV_{\mathrm{dc}mn}$, which can be adjusted as well to satisfy the system requirement.

The grid voltages (v_{mO}, $m = a, b, c$) and the phase currents (i_m, $m = a, b, c$) are likewise sensed and processed to draw out their sequence components. Defining ω as the grid frequency, they can be expressed as (1) and (2) shown at the bottom of this page, where p and n denote positive sequence and negative sequence, and q and d denote active axis and reactive axis. In addition, there is the freedom of the zero sequence voltage, whose usage will be investigated in the following section.

III. Power Flow Analysis

The power flow analysis on the HCC is a key point for the design of the proposed control scheme, so it needs to be discussed first. The power flow analysis relies on the information defined in (1) and (2), and also the usage of the zero sequence voltage. The zero sequence voltages for the H-bridge cells (v_H^0) and the two-level cell (v_T^0) are assumed as

$$v_H^0 = V_H^0 \cos(\omega t + \gamma_H^0) \tag{3}$$

$$v_T^0 = V_T^0 \cos(\omega t + \gamma_T^0) \tag{4}$$

where V_H^0 and V_T^0 indicate their respective amplitudes, and γ_H^0 and γ_T^0 indicate their respective phase angles.

Generally, the voltage references are shared among the cells with respect to the dc voltage utilization of the H-bridge cells ($V_{\mathrm{dc}mn}$) and the two-level cell ($1.15\mathrm{V}_{\mathrm{dc}N}/2$). The reason for the additional 1.15 times in the dc voltage utilization of the two-level cell will be clarified afterwards.

Fig. 3 shows the schematic diagram of the power flows in the HCC. If the voltage drop across the filter inductor (L_{ac}) is negligible, then the power flows in the H-bridge cells and the two-level cell, as shown in Fig. 3, can be derived as follows.

$$\begin{bmatrix} v_{aO} \\ v_{bO} \\ v_{cO} \end{bmatrix} = \begin{bmatrix} 1 & 0 \\ -\frac{1}{2} & -\frac{\sqrt{3}}{2} \\ -\frac{1}{2} & \frac{\sqrt{3}}{2} \end{bmatrix} \begin{bmatrix} v_\alpha \\ v_\beta \end{bmatrix} = \begin{bmatrix} 1 & 0 \\ -\frac{1}{2} & -\frac{\sqrt{3}}{2} \\ -\frac{1}{2} & \frac{\sqrt{3}}{2} \end{bmatrix} \begin{bmatrix} \cos(\omega t) & \sin(\omega t) \\ -\sin(\omega t) & \cos(\omega t) \end{bmatrix} \begin{bmatrix} V_q^p \\ V_d^p \end{bmatrix} + \begin{bmatrix} 1 & 0 \\ -\frac{1}{2} & -\frac{\sqrt{3}}{2} \\ -\frac{1}{2} & \frac{\sqrt{3}}{2} \end{bmatrix} \begin{bmatrix} \cos(\omega t) & -\sin(\omega t) \\ \sin(\omega t) & \cos(\omega t) \end{bmatrix} \begin{bmatrix} V_q^n \\ V_d^n \end{bmatrix} \tag{1}$$

$$\begin{bmatrix} i_a \\ i_b \\ i_c \end{bmatrix} = \begin{bmatrix} 1 & 0 \\ -\frac{1}{2} & -\frac{\sqrt{3}}{2} \\ -\frac{1}{2} & \frac{\sqrt{3}}{2} \end{bmatrix} \begin{bmatrix} i_\alpha \\ i_\beta \end{bmatrix} = \begin{bmatrix} 1 & 0 \\ -\frac{1}{2} & -\frac{\sqrt{3}}{2} \\ -\frac{1}{2} & \frac{\sqrt{3}}{2} \end{bmatrix} \begin{bmatrix} \cos(\omega t) & \sin(\omega t) \\ -\sin(\omega t) & \cos(\omega t) \end{bmatrix} \begin{bmatrix} I_q^p \\ I_d^p \end{bmatrix} + \begin{bmatrix} 1 & 0 \\ -\frac{1}{2} & -\frac{\sqrt{3}}{2} \\ -\frac{1}{2} & \frac{\sqrt{3}}{2} \end{bmatrix} \begin{bmatrix} \cos(\omega t) & -\sin(\omega t) \\ \sin(\omega t) & \cos(\omega t) \end{bmatrix} \begin{bmatrix} I_q^n \\ I_d^n \end{bmatrix} \tag{2}$$

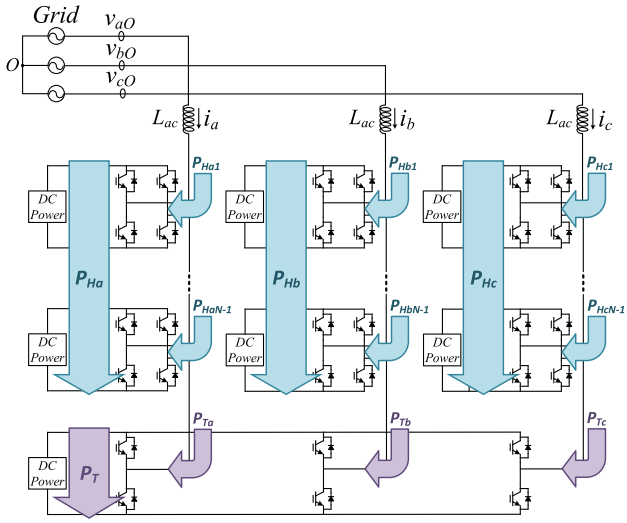

Fig. 3. Schematic diagram of the power flows in the HCC.

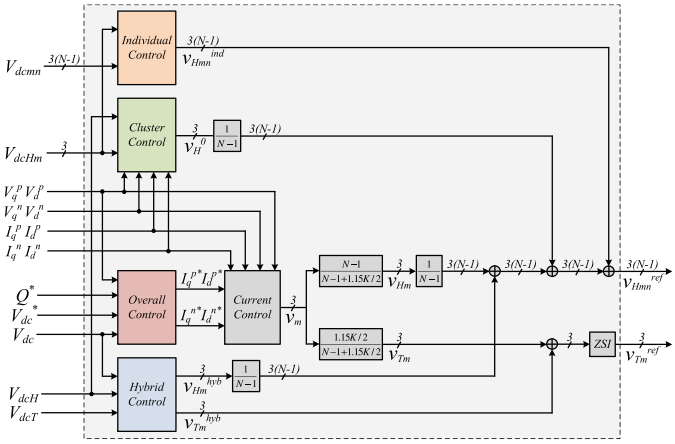

Fig. 4. Block diagram of the proposed control scheme.

A. Power Flows in the H-Bridge Cells

The phase power flow in the H-bridge cells (P_{Hm}) can be derived as

$$\begin{aligned} P_{Hm} &= P_{Hm1} + \cdots + P_{HmN-1} \\ &= \frac{\omega}{2\pi}\int_0^{\frac{2\pi}{\omega}} \left(\frac{N-1}{N-1+1.15K/2} v_{mO} + v_H^0\right)\cdot i_m \, dt \\ &= P_H/3 + P_{CHm} \end{aligned} \tag{5}$$

where $P_H = P_{Ha} + P_{Hb} + P_{Hc}$ and $P_{CHm} = P_{Hm} - P_H/3$. As can be seen, P_{Hm} essentially comprises its evenly shared overall power flow ($P_H/3$) and its probable unbalanced cluster power flow (P_{CHm}).

B. Power Flows in the Two-Level Cell

The phase power flow in the two-level cell (P_{Tm}) can be derived in the same manner as

$$\begin{aligned} P_{Tm} &= \frac{\omega}{2\pi}\int_0^{\frac{2\pi}{\omega}} \left(\frac{1.15K/2}{N-1+1.15K/2} v_{mO} + v_T^0\right)\cdot i_m \, dt \\ &= P_T/3 + P_{CTm} \end{aligned} \tag{6}$$

where $P_T = P_{Ta} + P_{Tb} + P_{Tc}$ and $P_{CTm} = P_{Tm} - P_T/3$. Similarly, P_{Tm} essentially comprises its evenly shared overall power flow ($P_T/3$) and its probable unbalanced cluster power flow (P_{CTm}). Somewhat differently, P_{Tm} should be concentrated in one capacitor. Thus, further summation of P_{Tm} is then derived as

$$P_{Ta} + P_{Tb} + P_{Tc} = P_T \ \left(\because P_{CTa} + P_{CTb} + P_{CTc} = 0\right) \tag{7}$$

which is exactly the overall power flow in the two-level cell.

It is worth noting that the probable unbalanced cluster power flows in the two-level cell disappear due to the power concentration in one capacitor. This characteristic points out that the control for managing the unbalanced power flows is demanded simply by the H-bridge cells.

IV. Proposed Control Scheme

Fig. 4 shows the block diagram of the proposed control scheme for the HCC to attain both the system current control and the dc capacitor voltage balancing control. With the power flow analysis given above, the proposed control scheme is designed and established in the four-layer hierarchical control structure shown in Fig. 2, in which the overall control, the cluster control, and the individual control come from [9] with a proper redesign for the HCC, while the hybrid control is a newly added control. Each control is explained as follows.

A. Overall Control

The overall control is to produce the current references required in the system to achieve the system current control. The current references ($I_q^{p*}, I_d^{p*}, I_q^{n*}, I_d^{n*}$) can be expressed as

$$I_q^{p*} = \left(K_p + \frac{K_i}{s}\right)\left(V_{\rm dc}^* - V_{\rm dc}\right), I_d^{p*} = \frac{2Q^*}{3V_q^p}, I_q^{n*} = I_d^{n*} = 0 \tag{8}$$

where $V_{\rm dc} = \frac{1}{2}\left[\frac{\sum_{n=1}^{N-1}(V_{\rm dcan}+V_{\rm dcbn}+V_{\rm dccn})}{3(N-1)} + \frac{V_{\rm dcN}}{K}\right]$.

I_q^{p*} is to control the active current to achieve the overall average dc capacitor voltage balancing, which is generated by regulating the error between the dc capacitor voltage command ($V_{\rm dc}^*$) and the average dc capacitor voltage ($V_{\rm dc}$) with a PI controller. I_d^{p*} is to control the reactive current according to the reactive power requirement (Q^*). I_q^{n*} and I_d^{n*} are to control the negative sequence current, and they are controlled to zero in this paper because the unbalanced currents are generally not desired at the utility grid.

The current references in (8) are then processed by the current control to produce the voltage references of the overall control (v_m), which are shared by the H-bridge cells (v_{Hm}) and the two-level cell (v_{Tm}).

B. Hybrid Control

The hybrid control is to manage the active power between the H-bridge cells and the two-level cell to achieve the average dc capacitor voltage balancing of themselves. The voltage references of the hybrid control for the H-bridge cells (v_{Hm}^{hyb}) and the two-level cell (v_{Tm}^{hyb}) can be expressed as

$$v_{Hm}^{\mathrm{hyb}} = \left(K_p^{\mathrm{hyb}} + \frac{K_i^{\mathrm{hyb}}}{s}\right)\left(V_{\mathrm{dc}} - V_{\mathrm{dc}H}\right)\cdot i_m \tag{9}$$

$$v_{Tm}^{\mathrm{hyb}} = \left(K_p^{\mathrm{hyb}} + \frac{K_i^{\mathrm{hyb}}}{s}\right)\left(V_{\mathrm{dc}} - V_{\mathrm{dc}T}\right)\cdot i_m \tag{10}$$

where $V_{\mathrm{dc}H} = \frac{\sum_{n=1}^{N-1}(V_{\mathrm{dc}an}+V_{\mathrm{dc}bn}+V_{\mathrm{dc}cn})}{3(N-1)}$ and $V_{\mathrm{dc}T} = \frac{V_{\mathrm{dc}N}}{K}$.

v_{Hm}^{hyb} and v_{Tm}^{hyb} are generated by regulating the error between the average dc capacitor voltage (V_{dc}) and the average dc capacitor voltage of themselves ($V_{\mathrm{dc}H}, V_{\mathrm{dc}T}$) with PI controllers, and then multiplying i_m to make sure that the voltage regulations are in phase with the phase currents.

C. Cluster Control

As discussed in [10], the cluster control can be carried out by means of the zero sequence voltage. However, from the summary of the power flow analysis on the HCC, it is known that the control for managing the unbalanced power flows, namely the cluster control, is demanded simply by the H-bridge cells. Consequently, only the zero sequence voltage for the H-bridge cells needs to be determined, as expressed in (3).

The cluster control is to manage the active power among different phase clusters of the H-bridge cells to achieve the average dc capacitor voltage balancing of each phase cluster of the H-bridge cells. Once the unbalanced power flows occur, the zero sequence voltage for the H-bridge cells is generated from the following derivation.

From (5), the probable unbalanced cluster power flow in the H-bridge cells (P_{CHm}) can be further rewritten as

$$P_{CHm} = P_{Hm} - \frac{P_H}{3} = P_{CHm}^{pn} + P_{CHm}^{0} \tag{12}$$

which is divided into P_{CHm}^{pn} containing its positive sequence voltage and negative sequence voltage, and P_{CHm}^{0} containing its zero sequence voltage. Since the zero sequence voltage required in the H-bridge cells can be calculated from P_{CHm}^{0} in (12), the cluster control is then designed as

$$P_{CHm}^{0} = P_{CHm} - P_{CHm}^{pn} = P_{CHm}^{FB} - P_{CHm}^{FF} \tag{13}$$

where P_{CHm} are defined as the feedback terms (P_{CHm}^{FB}) because they are the real-time information and P_{CHm}^{pn} are defined as the feedforward terms (P_{CHm}^{FF}) because they are the known information. P_{CHm}^{FB} can be expressed as

$$P_{CHm}^{FB} = \left(K_p^{C} + \frac{K_i^{C}}{s}\right)\left(V_{\mathrm{dc}H} - V_{\mathrm{dc}Hm}\right) \tag{14}$$

where $V_{\mathrm{dc}Hm} = \frac{\sum_{n=1}^{N-1} V_{\mathrm{dc}mn}}{N-1}$. P_{CHm}^{FB} are generated by regulating the error between the average dc capacitor voltage of all the H-bridge cells ($V_{\mathrm{dc}H}$) and the average dc capacitor voltage of the H-bridge cells at the same phase ($V_{\mathrm{dc}Hm}$) with PI controllers. Also, P_{CHm}^{FF} can be derived by solving the aforementioned equations as (11) shown at the bottom of this page.

Eventually, P_{CHm}^{0} are transformed to $\alpha\beta$ frame because $P_{CHa}^{0} + P_{CHb}^{0} + P_{CHc}^{0} = 0$, and the relationships with the zero sequence voltage required in the H-bridge cells are

$$\begin{aligned}\begin{bmatrix} P_{CH\alpha}^{0} \\ P_{CH\beta}^{0} \end{bmatrix} &= \frac{2}{3}\begin{bmatrix} 1 & -\frac{1}{2} & -\frac{1}{2} \\ 0 & -\frac{\sqrt{3}}{2} & \frac{\sqrt{3}}{2} \end{bmatrix}\begin{bmatrix} P_{CHa}^{0} \\ P_{CHb}^{0} \\ P_{CHc}^{0} \end{bmatrix} \\ &= \frac{1}{2}\begin{bmatrix} I_q^p + I_q^n & I_d^n - I_d^p \\ I_d^p + I_d^n & I_q^p - I_q^n \end{bmatrix}\begin{bmatrix} V_H^0\cos(\gamma_H^0) \\ V_H^0\sin(\gamma_H^0) \end{bmatrix} \\ &\Longrightarrow v_H^0 = V_H^0\cos(\omega t + \gamma_H^0)\end{aligned} \tag{15}$$

where the zero sequence voltage for the H-bridge cells (v_H^0) can thus be obtained with its amplitude (V_H^0) and phase angle (γ_H^0).

D. Individual Control

The individual control is to manage the active power among the H-bridge cells at the same phase to achieve the dc capacitor voltage balancing of each H-bridge cell at the same phase. Similar to the concept of the hybrid control, the voltage references of the individual control for each H-bridge cell at the same phase (v_{Hmn}^{ind}) can be expressed as

$$v_{Hmn}^{\mathrm{ind}} = \left(K_p^{\mathrm{ind}} + \frac{K_i^{\mathrm{ind}}}{s}\right)\left(V_{\mathrm{dc}Hm} - V_{\mathrm{dc}mn}\right)\cdot i_m. \tag{16}$$

v_{Hmn}^{ind} are generated by regulating the error between the average dc capacitor voltage of the H-bridge cells at the same phase ($V_{\mathrm{dc}Hm}$) and the dc capacitor voltage of each H-bridge cell at the same phase ($V_{\mathrm{dc}mn}$) with PI controllers, and then multiplying i_m to make sure that the voltage regulations are in phase with the phase currents.

$$\begin{aligned}
P_{CHa}^{FF} &= \frac{N-1}{N-1+1.15K/2}\left[\frac{1}{2}\left(V_q^n I_q^p - V_d^n I_d^p + V_q^p I_q^n - V_d^p I_d^n\right)\right] \\
P_{CHb}^{FF} &= \frac{N-1}{N-1+1.15K/2}\left[\frac{-1}{4}\left(V_q^n I_q^p - V_d^n I_d^p + V_q^p I_q^n - V_d^p I_d^n\right) + \frac{\sqrt{3}}{4}\left(V_q^n I_d^p + V_d^n I_q^p + V_q^p I_d^n + V_d^p I_q^n\right)\right] \\
P_{CHc}^{FF} &= \frac{N-1}{N-1+1.15K/2}\left[\frac{-1}{4}\left(V_q^n I_q^p - V_d^n I_d^p + V_q^p I_q^n - V_d^p I_d^n\right) + \frac{-\sqrt{3}}{4}\left(V_q^n I_d^p + V_d^n I_q^p + V_q^p I_d^n + V_d^p I_q^n\right)\right]
\end{aligned} \tag{11}$$

By summing together the voltage references from all of the controls described above, the final voltage references for the H-bridge cells (v_{Hmn}^{ref}) and the two-level cell (v_{Tm}^{ref}) can be obtained as

$$v_{Hmn}^{\mathrm{ref}} = \frac{v_{Hm}}{N-1} + \frac{v_{Hm}^{\mathrm{hyb}}}{N-1} + \frac{v_H^0}{N-1} + v_{Hmn}^{\mathrm{ind}} \tag{17}$$

$$v_{Tm}^{\mathrm{ref}} = v_{Tm} + v_{Tm}^{\mathrm{hyb}} + \mathrm{ZSI}. \tag{18}$$

Since the zero sequence voltage expressed in (4) is not used, another freedom of zero sequence voltage remains in the two-level cell. Thus, in this paper, the zero sequence injection (ZSI) discussed in [17] is further used in (18) to improve the output performance, which can be expressed as

$$\mathrm{ZSI} = -\frac{\max\left(v_{Tm} + v_{Tm}^{\mathrm{hyb}}\right) + \min\left(v_{Tm} + v_{Tm}^{\mathrm{hyb}}\right)}{2}. \tag{19}$$

Moreover, the ZSI can inherently help the dc voltage utilization increase by 1.15 times [17], which is why the two-level cell is able to share some more voltage references.

v_{Hmn}^{ref} and v_{Tm}^{ref} are then processed by the well-known phase-shifted PWM (PSPWM) [18] to produce the gate signals for the H-bridge cells and the two-level cell. The implementation of the PSPWM has been explained in detail in [9]; therefore, this paper makes no description on it.

V. Comparison Between the HCC and the SSBC Under Unbalanced Conditions

Thanks to the zero sequence voltage, the HCC is allowed to continue operating even under unbalanced conditions. Unfortunately, injecting the zero sequence voltage increases the risk of overmodulation, which may lead to an unstable system operation. This section attempts to compare the zero sequence voltage requirement of the HCC with that of the SSBC under the same unbalanced conditions to evaluate whether the HCC is a competitive candidate. Note that this paper takes the amplitude of the zero sequence voltage as the criterion of the zero sequence voltage requirement.

Assuming that the negative sequence currents are controlled to zero, the zero sequence voltage for the HCC (v_H^0) can be derived from (15) and its amplitude (V_H^0) can be calculated as (20) shown at the bottom of this page. Besides, the zero sequence voltage for the SSBC (v^0) can be derived from [10] and its amplitude (V^0) can be calculated as (21) shown at the bottom of this page. P_{CHm} and P_{Cm} can be regarded as the unbalanced powers at dc-side, and P_{CHm}^{pn} and P_{Cm}^{pn} can be regarded as the unbalanced powers at ac-side. Their relationships are

$$P_{CHm} = P_{Cm},\ P_{CHm}^{pn} = \left(\frac{N-1}{N-1+1.15K/2}\right) P_{Cm}^{pn} \tag{22}$$

which means that V_H^0 is equal to V^0 under the same unbalanced conditions at dc-side, but V_H^0 is less than V^0 under the same unbalanced conditions at ac-side.

The above-obtained results are summarized as follows.

1) Zero sequence voltage requirement under unbalanced conditions at dc-side: HCC = SSBC.
2) Zero sequence voltage requirement under unbalanced conditions at ac-side: HCC < SSBC.

It is found that the HCC has relatively lighter burden under unbalanced conditions at ac-side than at dc-side. Therefore, the HCC is expected to be more reliable under unbalanced conditions at ac-side than at dc-side.

TABLE I
Testbench Parameters

	Value
Grid voltage (L-L rms)	220(V)
Grid frequency	60(Hz)
AC filter inductor	6.8(mH)
Nominal DC voltage (H-bridge cells)	80(V)
Nominal DC voltage (two-level cell)	160(V)
Unit capacitance constant [19]	43.59(msec)
Switching frequency	2(kHz)
Sampling frequency	12(kHz)

VI. Laboratory Test Results

To verify the proposed control scheme, the laboratory test results are illustrated in this section. The testbench is built in the laboratory as the system configuration shown in Fig. 2 with the cascaded cell number $N = 3$ and the dc voltage ratio $K = 2$. The corresponding system parameters are given in Table I.

In this paper, the dc powers are simulated by connecting all the cells with resistors, and the additional switches are added to realize the sudden power variation at dc-side. In addition, the grid faults are also simulated by implementing voltage sag on the system to realize the asymmetrical grid voltages at ac-side, and meanwhile, 500 Var reactive power is injected into the grid ($Q^* = -500$ Var) to support the grid.

$$\begin{bmatrix} P_{CH\alpha}^0 \\ P_{CH\beta}^0 \end{bmatrix} = \frac{2}{3}\begin{bmatrix} 1 & -\frac{1}{2} & -\frac{1}{2} \\ 0 & -\frac{\sqrt{3}}{2} & \frac{\sqrt{3}}{2} \end{bmatrix}\begin{bmatrix} P_{CHa} - P_{CHa}^{pn} \\ P_{CHb} - P_{CHb}^{pn} \\ P_{CHc} - P_{CHc}^{pn} \end{bmatrix} \Longrightarrow V_H^0 = \frac{2}{\sqrt{(I_q^p)^2 + (I_d^p)^2}}\sqrt{(P_{CH\alpha}^0)^2 + (P_{CH\beta}^0)^2} \tag{20}$$

$$\begin{bmatrix} P_{C\alpha}^0 \\ P_{C\beta}^0 \end{bmatrix} = \frac{2}{3}\begin{bmatrix} 1 & -\frac{1}{2} & -\frac{1}{2} \\ 0 & -\frac{\sqrt{3}}{2} & \frac{\sqrt{3}}{2} \end{bmatrix}\begin{bmatrix} P_{Ca} - P_{Ca}^{pn} \\ P_{Cb} - P_{Cb}^{pn} \\ P_{Cc} - P_{Cc}^{pn} \end{bmatrix} \Longrightarrow V^0 = \frac{2}{\sqrt{(I_q^p)^2 + (I_d^p)^2}}\sqrt{(P_{C\alpha}^0)^2 + (P_{C\beta}^0)^2} \tag{21}$$

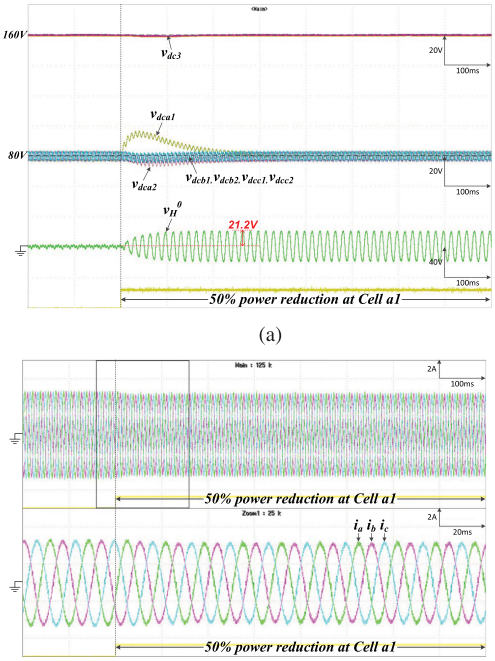

Fig. 5. Waveforms tested under the unbalanced condition of 50% power reduction at $Cell\ a1$. (a) DC capacitor voltages and the zero sequence voltage for the H-bridge cells. (b) Phase currents.

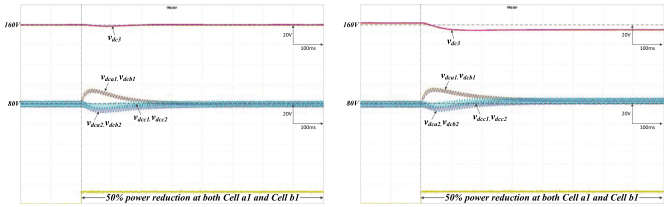

Fig. 6. Waveforms tested under the unbalanced condition of 50% power reduction at both $Cell\ a1$ and $Cell\ b1$. (a) DC capacitor voltages. (b) DC capacitor voltages using the controller without the hybrid control.

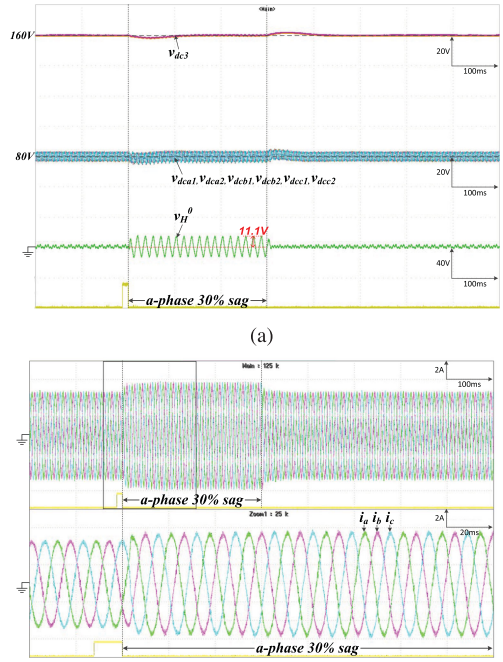

Fig. 7. Waveforms tested under the unbalanced condition of 30% voltage sag at $a\text{-}phase$. (a) DC capacitor voltages and the zero sequence voltage for the H-bridge cells. (b) Phase currents.

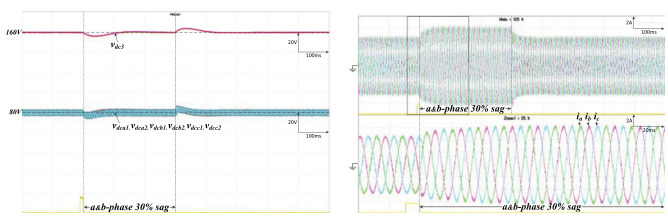

Fig. 8. Waveforms tested under the unbalanced condition of 30% voltage sag at both $a\text{-}phase$ and $b\text{-}phase$. (a) DC capacitor voltages. (b) Phase currents.

Under normal operation, each H-bridge cell is connected with a 50-Ω resistor and the two-level cell is connected with a 75-Ω resistor, which means that the system operates at about 1.11 kW rated power. The system is then tested under the following unbalanced conditions.

A. Tested Under Unbalanced Conditions at DC-Side

Fig. 5 illustrates the waveforms tested under the unbalanced condition of 50% power reduction at $Cell\ a1$ by increasing its resistor to 100 Ω. Fig. 5(a) shows that the dc capacitor voltages of the H-bridge cells and the two-level cell can be well controlled after 50% power reduction at $Cell\ a1$ because of the zero sequence voltage for the H-bridge cells (v_H^0). Fig. 5(b) shows that the phase currents can be controlled balanced after 50% power reduction at $Cell\ a1$ because the negative sequence currents are controlled to zero.

The waveforms tested under the unbalanced condition of 50% power reduction at both $Cell\ a1$ and $Cell\ b1$ by increasing their resistors to 100 Ω are illustrated in Fig. 6(a) as well. Additionally, under this unbalanced condition, the controller without the hybrid control is also tested, and the waveforms are illustrated in Fig. 6(b). Obviously, the dc capacitor voltages of the H-bridge cells and the two-level cell deviate from 80 V and 160 V, which clarifies the importance of the hybrid control.

B. Tested Under Unbalanced Conditions at AC-Side

Fig. 7 illustrates the waveforms tested under the unbalanced condition of 30% voltage sag at $a\text{-}phase$. Fig. 7(a) shows that the dc capacitor voltages of the H-bridge cells and the two-level cell can be well controlled during 30% voltage sag at $a\text{-}phase$ because of the zero sequence voltage for the H-bridge cells (v_H^0). Fig. 7(b) shows that the phase currents can be controlled balanced during 30% voltage sag at $a\text{-}phase$ because the negative sequence currents are controlled to zero.

The waveforms tested under the unbalanced condition of 30% voltage sag at both $a\text{-}phase$ and $b\text{-}phase$ are illustrated in Fig. 8,

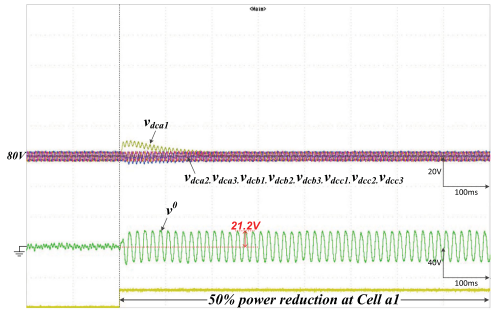

(a)

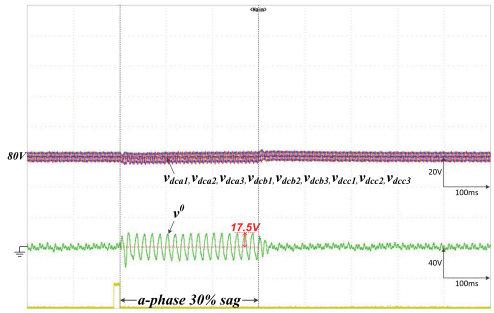

(b)

Fig. 9. Waveforms tested on the SSBC. (a) Unbalanced condition of 50% power reduction at $Cell\ a1$. (b) Unbalanced condition of 30% voltage sag at $a\text{-}phase$.

where the well-controlled dc capacitor voltages and the balanced phase currents can also be observed in Fig. 8(a) and (b).

C. Compared With the SSBC Under Unbalanced Conditions

In order to verify the comparison in Section V, the SSBC with the cascaded cell number $N = 3$ is built in the laboratory as well, and the system parameters are identical to those of the HCC. The SSBC is also tested under the unbalanced condition of 50% power reduction at $Cell\ a1$ and the unbalanced condition of 30% voltage sag at $a\text{-}phase$, and the waveforms are illustrated in Fig. 9.

Comparing Figs. 5(a) and 7(a) with Fig. 9(a) and (b), it can be found that the zero sequence voltages required in the HCC and the SSBC agree with the comparative results summarized in Section V, which once again demonstrates that the HCC has more alleviated burden under unbalanced conditions at ac-side than at dc-side, as highlighted in Section V.

VII. Discussion

In this section, the operating boundaries of the HCC and the SSBC based on the unbalanced operations in Section VI are investigated. Following the findings, this section would like to look for the most suitable grid application of the HCC and also its operational flexibility and reliability.

In Section VI, the modulation index (M) is intentionally overdesigned out of safety concerns, yet in this section, $M = 0.8$ is set for the normal operation (without injecting the zero sequence voltage) and $M = 1.0$ is set for the operating boundary (overmodulation). Note that the overmodulation is also related to

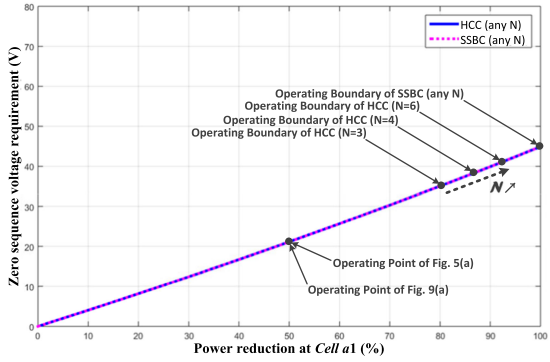

(a)

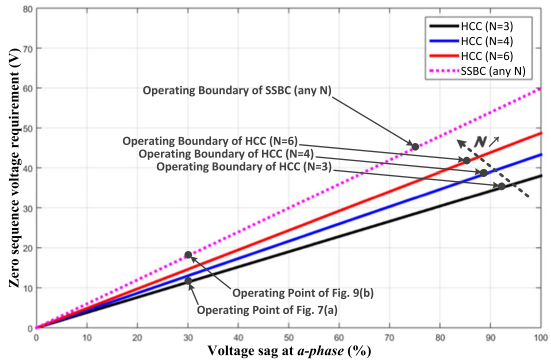

(b)

Fig. 10. Graphs of the zero sequence voltage requirements under the unbalanced operations of (a) power reduction at $Cell\ a1$ from 0% to 100% and (b) voltage sag at $a\text{-}phase$ from 0% to 100%, with $K = 2$.

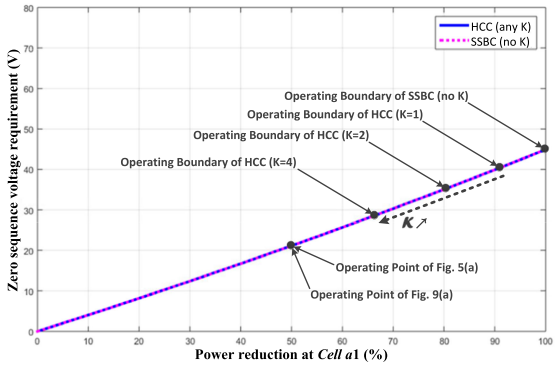

(a)

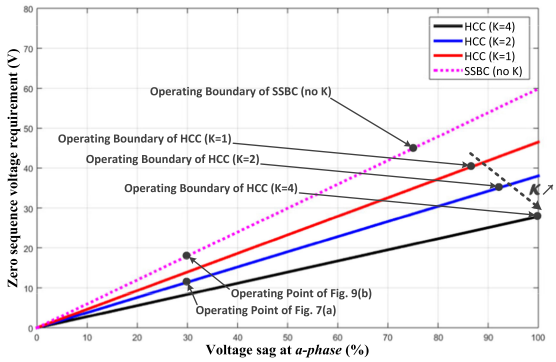

(b)

Fig. 11. Graphs of the zero sequence voltage requirements under the unbalanced operations of (a) power reduction at $Cell\ a1$ from 0% to 100% and (b) voltage sag at $a\text{-}phase$ from 0% to 100%, with $N = 3$.

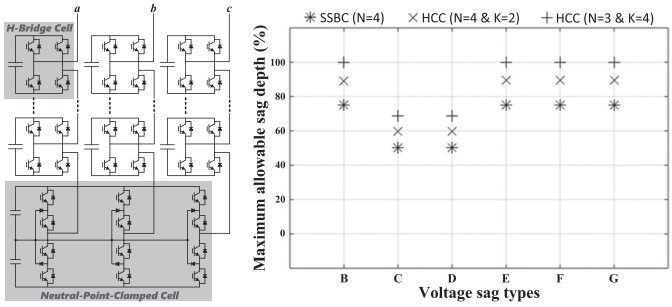

(a) (b)

Fig. 12. Supplementary information. (a) Alternative HCC. (b) Maximum allowable sag depths under different voltage sag types.

the phase angle of the injected zero sequence voltage, whereas it is ignored in this section for easier observation on the operating boundary.

Based on (20)–(22), the graphs of the zero sequence voltage requirements under the unbalanced operations in Section VI with varying severity are illustrated in Fig. 10 (with K fixed) and Fig. 11 (with N fixed), in which the operating boundaries are plotted, and the operating points in Section VI are depicted as well to confirm that the laboratory test results are performed in accordance with the graphs. As can be seen, the severer the unbalanced operations, the larger the zero sequence voltage requirements, and hence the superiority of the HCC under the unbalanced operations at ac-side becomes more significant. In addition, the operating boundaries of the HCC under the unbalanced operations at ac-side can be further improved by decreasing N, as shown in Fig. 10(b), or increasing K, as shown in Fig. 11(b), which cannot be achieved in Figs. 10(a) and 11(a) no matter how N/K changes.

On the basis of the above findings, it may be said that the HCC is a more suitable STATCOM candidate than the SSBC to deal with the unbalanced grid conditions and fault ride through requirements [6]–[10]. For better understanding of its operational flexibility and reliability, several possible designs for the 6.6 kV full-scale STATCOM are given as follows.

1) The SSBC with $N = 4$ is applied. The 3300 V IGBTs are used for twelve H-bridge cells. The maximum allowable single-phase sag depth is 75% [see Fig. 10(b) dotted line].
2) The HCC with $N = 4$ and $K = 2$ is applied. The 3300 V and 6500 V IGBTs are used for nine H-bridge cells and one two-level cell, respectively. The maximum allowable single-phase sag depth is 89% [see Fig. 10(b) blue line].
3) The HCC with $N = 3$ and $K = 4$ is applied. The 3300 V and 12 kV IGBTs are used for six H-bridge cells and one two-level cell, respectively. The maximum allowable single-phase sag depth is 100% [see Fig. 11(b) black line].

Obviously, the HCC performs much better than the SSBC, and further improvement can be achieved by decreasing N and increasing K. Although the required total power devices are reduced, the power devices with higher blocking voltage are requested for the two-level cell. For this reason, an alternative HCC is provided in Fig. 12(a) to adapt to the modification. Moreover, besides the single-phase voltage sag (Type B), other different voltage sag types are taken into consideration as well to make the above-mentioned more convincing, as shown in Fig. 12(b). Note that Type A is not involved because it is the three-phase balanced voltage sag.

VIII. Conclusion

This paper presents a hierarchical control scheme for the HCC in grid applications to fulfill both the system current control and the dc capacitor voltage balancing control. The proposed control scheme is capable of effectively managing the power flows in the HCC. Even under unbalanced conditions, all the dc capacitor voltages can still be maintained without affecting the system operation. The laboratory test results are illustrated, and they validate the effectiveness of the proposed control scheme. Furthermore, the HCC is compared with the SSBC under unbalanced conditions, and the comparative results show that the HCC has better performance under unbalanced conditions at ac-side than at dc-side. Owing to this characteristic, the HCC is expected to be more suitable for STATCOM than for RES or BESS.

References

[1] H. Akagi, "Classification, terminology, and application of the modular multilevel cascade converter (MMCC)," *IEEE Trans. Power Electron.*, vol. 26, no. 11, pp. 3119–3130, Nov. 2011.
[2] Y. Yu, G. Konstantinou, B. Hredzak, and V. G. Agelidis, "Power balance of cascaded H-bridge multilevel converters for large-scale photovoltaic integration," *IEEE Trans. Power Electron.*, vol. 31, no. 1, pp. 292–303, Jan. 2016.
[3] B. Xiao, L. Hang, J. Mei, C. Riley, L. M. Tolbert, and B. Ozpineci, "Modular cascaded H-bridge multilevel PV inverter with distributed MPPT for grid-connected applications," *IEEE Trans. Industry Appl.*, vol. 51, no. 2, pp. 1722–1731, Mar. 2015.
[4] Y. Yu, G. Konstantinou, B. Hredzak, and V. G. Agelidis, "Power balance optimization of cascaded H-bridge multilevel converters for large-scale photovoltaic integration," *IEEE Trans. Power Electron.*, vol. 31, no. 2, pp. 1108–1120, Feb. 2016.
[5] L. Maharjan, S. Inoue, H. Akagi, and J. Asakura, "State-of-charge (SoC)-balancing control of a battery energy storage system based on a cascade PWM converter," *IEEE Trans. Power Electron.*, vol. 24, no. 6, pp. 1628–1636, Jun. 2009.
[6] C. T. Lee *et al.*, "Average power balancing control of a STATCOM based on the cascaded H-bridge PWM converter with star configuration," *IEEE Trans. Ind. Appl.*, vol. 50, no. 6, pp. 3893–3901, Nov. 2014.
[7] B. Gultekin and M. Ermis, "Cascaded multilevel converter-based transmission STATCOM: System design methodology and development of a 12 kV ± 12 MVAr power stage," *IEEE Trans. Power Electron.*, vol. 28, no. 11, pp. 4930–4950, Nov. 2013.
[8] K. Sano and M. Takasaki, "A transformerless D-STATCOM based on a multivoltage cascade converter requiring no dc sources," *IEEE Trans. Power Electron.*, vol. 27, no. 6, pp. 2783–2795, Jun. 2012.
[9] H. Akagi, S. Inoue, and T. Yoshii, "Control and performance of a transformerless cascade PWM STATCOM with star configuration," *IEEE Trans. Ind. Appl.*, vol. 43, no. 4, pp. 1041–1049, Jul. 2007.
[10] H. C. Chen, P. H. Wu, C. T. Lee, C. W. Wang, C. H. Yang, and P. T. Cheng, "Zero-sequence voltage injection for dc capacitor voltage balancing control of the star-connected cascaded H-bridge PWM converter under unbalanced grid," *IEEE Trans. Ind. Appl.*, vol. 51, no. 6, pp. 4584–4594, Nov. 2015.
[11] J. Wen and K. M. Smedley, "Synthesis of multilevel converters based on single- and/or three-phase converter building blocks," *IEEE Trans. Power Electron.*, vol. 23, no. 3, pp. 1247–1256, May 2008.
[12] S. Mekhilef and M. N. A. Kadir, "Novel vector control method for three-stage hybrid cascaded multilevel inverter," *IEEE Trans. Ind. Electron.*, vol. 58, no. 4, pp. 1339–1349, Apr. 2011.

[13] S. Khomfoi, N. Praisuwanna, and L. M. Tolbert, "A hybrid cascaded multilevel inverter application for renewable energy resources including a reconfiguration technique," in *Proc. IEEE Energy Convers. Congr. Expo.*, Sep. 2010, pp. 3998–4005.
[14] Y. Zhang, G. Adam, S. Finney, and B. Williams, "Improved pulse-width modulation and capacitor voltage-balancing strategy for a scalable hybrid cascaded multilevel converter," *IET Power Electron.*, vol. 6, no. 4, pp. 783–797, Apr. 2013.
[15] A. Felinto, C. B. Jacobina, E. L. L. Fabricio, V. F. M. B. Melo, and J. P. R. A. Mello, "Investigation of power rectifier under non-sinusoidal input based on hybrid multilevel converter," in *Proc. IEEE Energy Convers. Congr. Expo.*, Oct. 2017, pp. 2779–2786.
[16] Y. C. Su, P. H. Wu, and P. T. Cheng, "Control of the hybrid cascaded converter under unbalanced conditions," in *Proc. IEEE Energy Convers. Congr. Expo.*, Oct. 2017, pp. 2858–2565.
[17] A. M. Hava, R. J. Kerkman, and T. A. Lipo, "Simple, analytical, and graphical methods for carrier-based PWM-VSI drives," *IEEE Trans. Power Electron.*, vol. 14, no. 1, pp. 49–61, Jan. 1999.
[18] Y. Li, Y. Wang, and B. Q. Li, "Generalized theory of phase-shifted carrier PWM for cascaded H-bridge converters and modular multilevel converters," *IEEE J. Emerg. Sel. Topics Power Electron.*, vol. 4, no. 2, pp. 589–605, Jun. 2016.
[19] H. Fujita, S. Tominaga, and H. Akagi, "Analysis and design of a dc voltage-controlled static VAr compensator using quad-series voltage-source inverters," *IEEE Trans. Ind. Appl.*, vol. 32, no. 4, pp. 970–978, Jul. 1996.

Yu-Chen Su (S'17) was born in Kaohsiung, Taiwan, in 1992. He received the B.S. degree, in 2015, from the Department of Electrical Engineering, National Tsing Hua University, Hsinchu, Taiwan, where he is currently working toward the Ph.D. degree.

His research interests include modular multilevel cascaded converters and their controls, modulations, and applications.

Ping-Heng Wu (S'13) was born in Taichung, Taiwan, in 1990. He received the B.S. degree in electrical engineering from National Chung Cheng University, Chiayi, Taiwan, in 2012, and the Ph.D. degree in electrical engineering at National Tsing Hua University, Hsinchu, Taiwan, in 2019.

He is currently an Engineer in power electronics for industry applications with Delta Electronics Inc., Taoyuan, Taiwan. His current research interests include modular multilevel cascaded converters in different applications and power converter controls.

Mr. Wu was a recipient of the International Conference on Power Electronics and IEEE Energy Conversion Congress and Exposition Best Paper Award in 2016.

Po-Tai Cheng (S'96–M'99–SM'09–F'18) received the B.S. degree from National Chiao Tung University, Hsinchu, Taiwan, in 1990, and the Ph.D. degree from the University of Wisconsin-Madison, Madison, WI, USA, in 1999.

He is currently a Professor with the Department of Electrical Engineering, National Tsing Hua University, Hsinchu. His research interests include high-power converters and applications, and power electronics technologies for smart grid.

Dr. Cheng was the recipient of the IAS Transactions Prize Paper Award in 2009 and IAS Industrial Power Converter Committee Paper Award in 2012 and 2014. He is the Chairperson of the Industrial Power Conversion Systems Department, IAS, 2016–2017, a Member-at-Large of the IAS Executive Board 2014–2015 and 2018, and the Chairperson of the Education Department, IAS 2019. He serves as a Distinguished Lecturer of IAS in 2019–2020 and of PELS in 2014–2017. He is currently an Associate Editor for IEEE TRANSACTIONS ON POWER ELECTRONICS.